JOURNAL OF MATERIALS SCIENCE 27 (1992) 3014–3020

Corrosion behaviour of a steel surface laser alloyed with chromium borides

YU ZUO*, R. M. LATANISION
Department of Materials Science and Engineering, Massachusetts Institute of Technology, Cambridge, MA 02139, USA

The corrosion behaviour of a carbon steel surface laser alloyed with chromium borides was investigated using electrochemical and surface analytical methods. Chromium and boron were unevenly distributed in the laser-alloyed layer. The distribution of chromium controlled the anodic dissolution of the alloy. Iron was dissolved preferentially from the surface and a loose corrosion product layer enriched in chromium was formed during active dissolution in 0.1 M H_2SO_4. The chromium boride inclusions on the surface promoted hydrogen evolution and controlled cathodic behaviour. In neutral and basic solutions, the corrosion behaviour of the laser-alloyed surface was very close to that of the matrix steel. The effects of the alloying elements on corrosion behaviour are discussed.

1. Introduction

It is well known that boronized steel has high hardness and good abrasion resistance. However, the structure and strength of the substrate steel may be affected by the conventional industrial boronizing process because of a relatively long heat-treatment time. In recent years, some authors [1–5] found that with a laser beam the surface can be alloyed with borides without affecting the substrate. Bamberger *et al.* [5] used a CO_2 laser to alloy the surface of AISI 1045 steel. CrB_2 powder was injected into the bath during the laser remelting processing. The chromium boride particles were partially dissolved in the bath, forming a melted layer of Fe–Cr–B–C. By this method an alloyed surface layer, with CrB_2 and Fe_2B as the main second phases, was formed, and exhibited a uniformly high hardness and very good abrasion resistance.

Moore and McCafferty [6] deposited a layer of chromium on AISI 1018 steel surface by electroplating or sputter depositing, and then remelted the surface using a laser beam. A chromium-alloyed surface layer was obtained by this method. The passivation ability of the material in 0.1 M Na_2SO_4 solution increased with increasing chromium content on the surface. It is interesting to note that in the present process the surface of 1045 steel is also alloyed with chromium. The presence of the chromium boride particles on the surface and the alloying of the surface by chromium and boron will affect electrochemical behaviour of the material. It may be expected that the corrosion resistance of the steel should be increased, because chromium is a passivation-promoting element. In the present work, the corrosion behaviour of a 1045 steel surface laser alloyed with CrB_2 was investigated to improve the understanding of environmental stability of surface-modified layers. Electrochemical techniques, SEM and electron microprobe, were used in the study.

2. Experimental procedure

The substrate material was 1045 steel. The surface was laser alloyed with CrB_2 (CO_2 laser of 1750 W, 2 mm beam diameter, 600 mm min^{-1} scanning velocity and 40% overlap). Fig. 1 shows the structure of the surface layer. The laser-remelted layer has a dendritic structure with a thickness of 400 μm on average. Beneath the surface layer the original structure (pearlite + ferrite) had been transformed to martensite due to the rapid cooling during laser treatment (Fig. 1a). There are many chromium boride particles left in the surface layer that were not melted during laser processing (Fig. 1b).

The samples were coated with two layers of epoxy resin to mask the untreated substrate. The surface of the samples were polished using 600 SiC abrasive paper and degreased in acetone. Untreated 1045 steel specimens were also used for comparison. Potentiodynamic polarization tests were carried out in nitrogen-deaerated solutions of 0.1 M H_2SO_4, 0.1 M Na_2SO_4 and 0.5 M NaOH which were prepared using reagent-grade chemicals and deionized water (18 MΩ cm). After immersion for 30 min in the test solution at open-circuit potential, the specimen was polarized cathodically at a potential of −400 mV relative to the open-circuit potential for 5 min, and was then polarized anodically with a scanning rate of 1 mV s^{-1}. Potential was measured with respect to a saturated calomel electrode. A galvanic couple test including the laser-alloyed surface and the matrix steel was carried out in sodium sulphate solution using a potentiostat, in order to reveal the electrochemical effect between the surface layer and the matrix. After

* *Present address*: Department of Applied Chemistry, Beijing Institute of Chemical Technology, Beijing 100029, China.

0022–2461

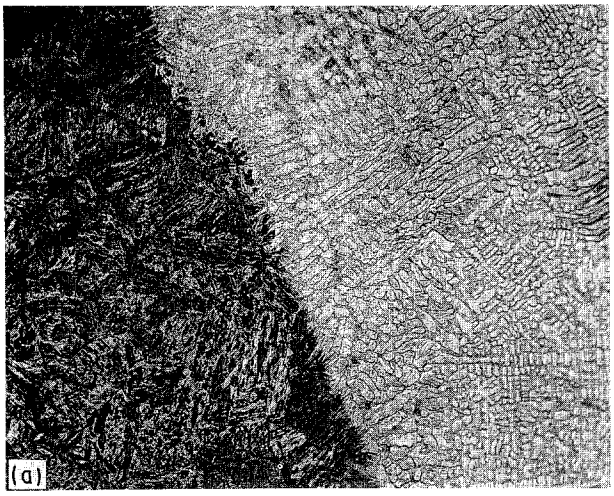

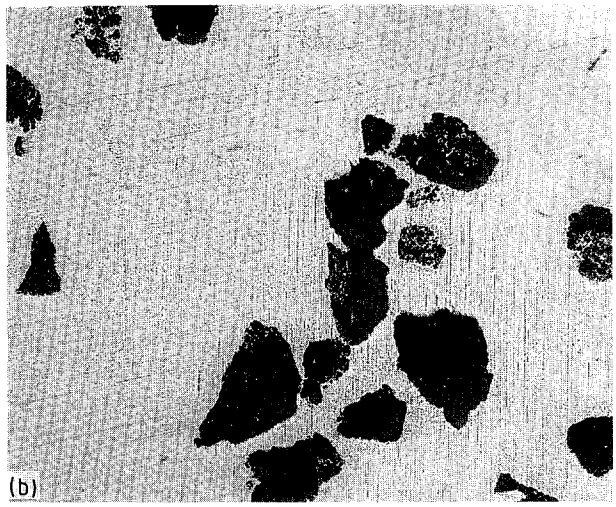

Figure 1 (a) Microstructures near the boundary between the laser treated surface layer and the matrix, × 200. (b) Chromium boride inclusions on the surface, × 100.

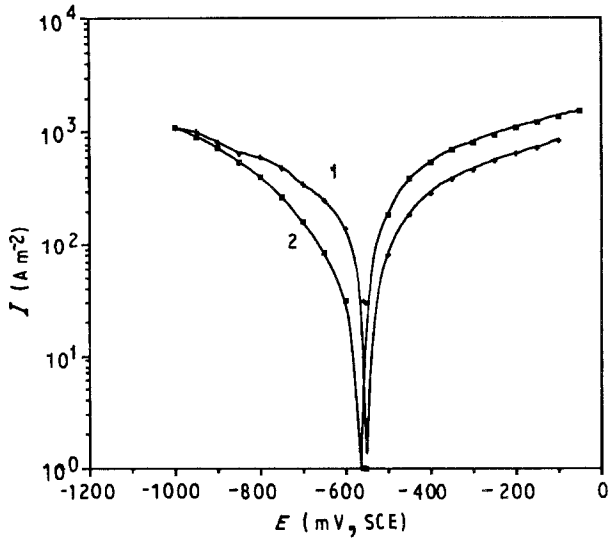

Figure 2 Polarization curves in 0.1 M H_2SO_4 solution, deaerated, at 25 °C.

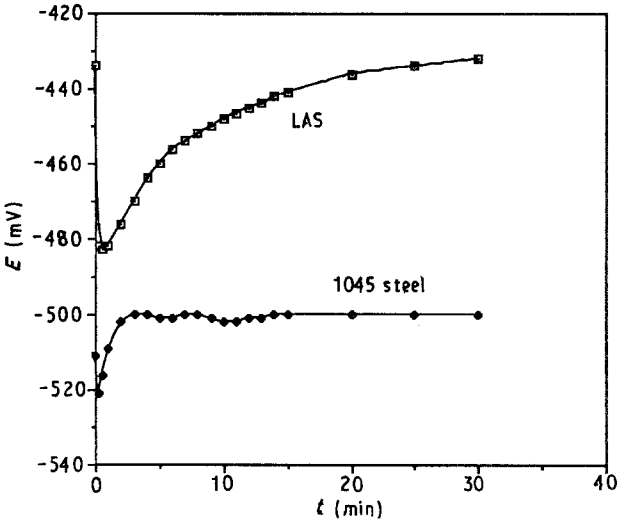

Figure 3 Open-circuit potential transient curves, in 0.1 M H_2SO_4, deaerated, at 25 °C.

electrochemical tests, the specimens were observed and analysed with an optical microscope, SEM and electron microprobe.

3. Results

Fig. 2 shows the polarization curve of the laser-alloyed surface (LAS) in 0.1 M H_2SO_4. The anodic portion of the curve shows an active dissolution without passivation. Compared to 1045 steel, the LAS has a higher cathodic current density at the same cathodic polarization potential. Tafel extrapolation indicates that the corrosion current density of the LAS is higher than that of 1045 steel. However, at anodic polarization potential, the anodic dissolution current is lower than that of 1045 steel. The polarization curve of unpolished surface is very close to that of a newly polished surface, indicating that there was no air-formed passive film on the laser-alloyed surface and the surface remained stable active dissolution in 0.1 M H_2SO_4.

Changes in corrosion potential of LAS in deaerated 0.1 M H_2SO_4 are shown as a function of time in Fig. 3. On immersion the corrosion potential shifted quickly in the negative direction from the initial value. However, this remained only for a few seconds and then the corrosion potential gradually moved in the positive direction. It took a relatively long time for LAS to establish a stable corrosion potential that is about 60 mV more positive than that of the matrix steel. In dilute sulphuric acid solution, the corrosion potential of Fe–Cr alloys decreased gradually as the chromium content in the alloy was increased [7]. Hence the increase of corrosion potential of the LAS is not the result of addition of chromium in the surface layer. Also, the dissolution rate and dissolution mechanism of iron were not influenced greatly by the addition of boron [8]. Therefore, the second-phase particles on the laser-alloyed surface seem responsible for the higher corrosion potential. During immersion of the sample at open-circuit potential, the evolution of bubbles from the surface of LAS was observed, which did not occur on the 1045 steel surface.

Fig. 4 shows the surface morphology of LAS specimen immersed in 0.1 M H_2SO_4 for 20 min at open-circuit potential. Regions around particles show different corrosion depths, and many pits can be seen on the

TABLE I Electron microprobe analysis results

Point	Fe		Cr		B	
	at %	wt %	at %	wt %	at %	wt %
A	0.15	0.27	48.78	81.65	51.08	18.09
B	62.17	70.99	24.55	26.03	13.28	2.98
C	86.75	91.17	7.92	7.73	5.33	1.10
D	94.38	96.06	3.78	3.57	1.84	0.37

surface. At anodic potentials, the difference in corrosion rates on different sections of the surface can be seen more clearly. Fig. 5a and b show surface morphologies of a polished LAS sample after it was polarized anodically 30 mV from the corrosion potential in 0.1 M H_2SO_4 for 30 s and 20 min, respectively. Apparently the different areas were corroded in different rates. Fig. 6 is a scanning electron micrograph of an area near a chromium boride particle. Pits can be seen clearly. Electron microprobe analysis reveals the composition difference of different areas (Table I). Point A is obviously a chromium boride inclusion, probably CrB. Point B is situated in the portion close to the inclusion. Points C and D are situated in the alloyed layer. The further from the chromium boride particle, the lower are the concentrations of chromium and boron. Therefore, it seems reasonable that the different corrosion rates are due to varying chromium contents. During anodic polarization, many pits were formed on the sections relatively far from chromium boride particles. Fig. 7 shows the morphology of these pits. The average diameter of the pits is about 1–2 μm. Some pits can be seen forming along the axis of the dendrites and it appears that some are going to merge. The chromium content of a polished LAS sample was analysed using electron microprobe and the results are shown in Table II. All the analysed points were situated in areas relatively far from chromium boride particles, but were selected randomly. Fig. 8 shows the chromium distribution along a randomly selected line on the surface. From these results we can see that chromium is not distributed evenly in the laser remelted surface but is concentrated at some spots. The reason for the uneven distribution of chromium is not clear, however, it may relate to the laser energy, the quenching velocity, the degree of overlap and the distribution of the chromium boride particles on the surface. It is conceivable that the pits come from preferential dissolution of active sites which are more enriched in iron and depleted of chromium. This is supported by the observation (Figs 4 and 6) that the axes of dendrites were corroded more easily, because they were enriched in iron during their solidification.

TABLE II Chromium contents at different points on the surface

Point	1	2	3	4	5	6	7
Cr (wt %)	4.11	5.50	4.21	3.03	3.66	4.20	3.38

However, after a relatively long time of anodic polarization, the pits disappeared and the surface was covered with a layer of corrosion products (Fig. 9). Fig. 10 shows the cross-section of a corroded sample

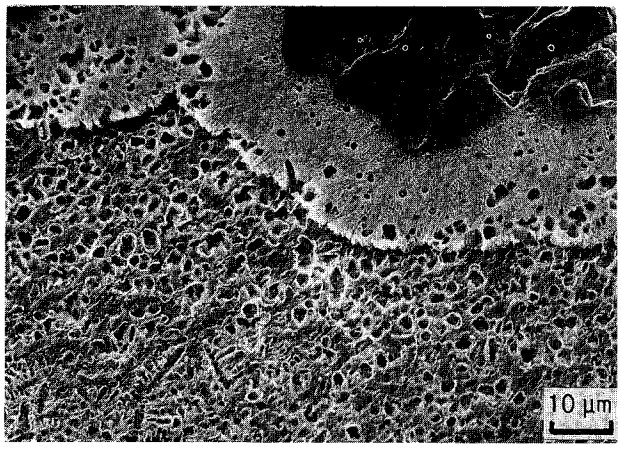

Figure 4 Surface morphology of LAS immersed in 0.1 M H_2SO_4 solution for 20 min at open-circuit potential.

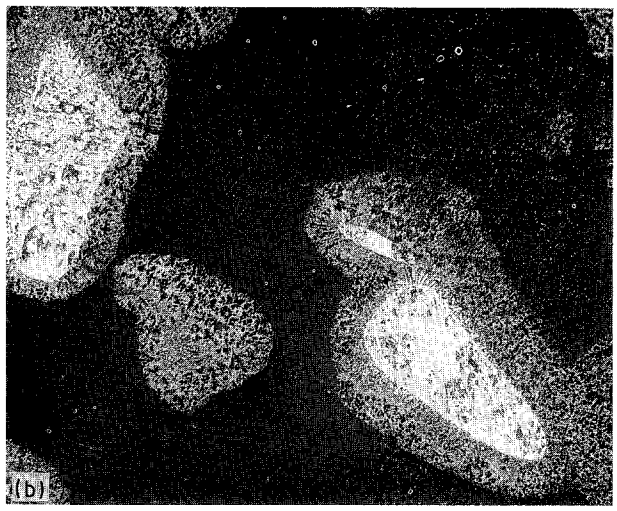

Figure 5 Surface morphology of LAS after polarization at a 30 mV anodic potential for (a) 30 s, × 100, (b) 20 min, × 200.

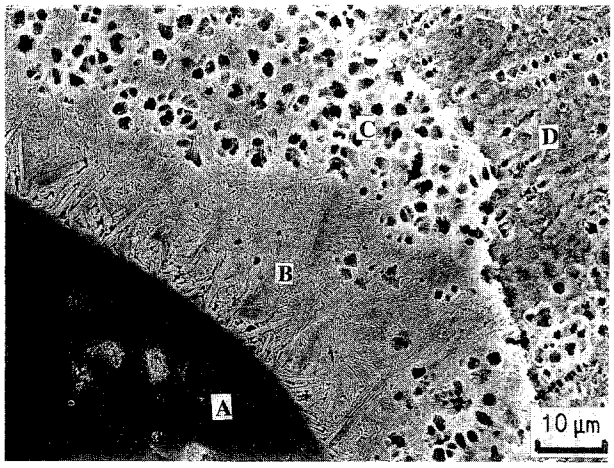

Figure 6 SEM morphology of LAS polarized at a 30 mV anodic potential for 20 min.

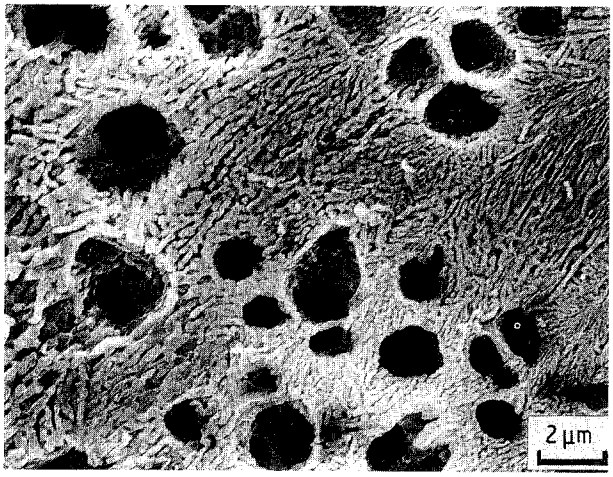

Figure 7 Morphology of the pits.

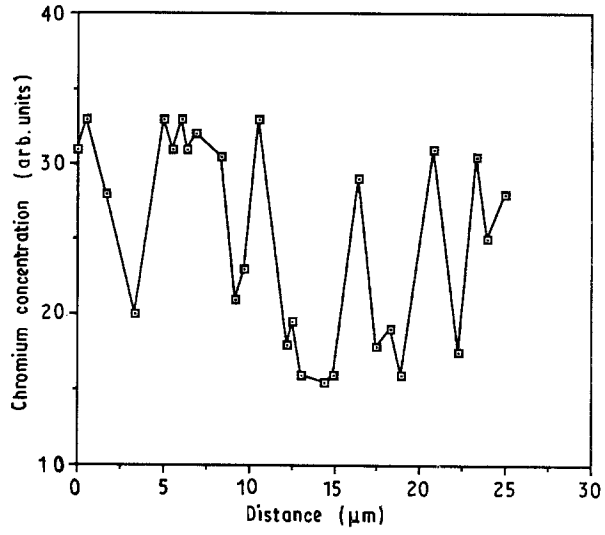

Figure 8 Distribution of chromium on the surface.

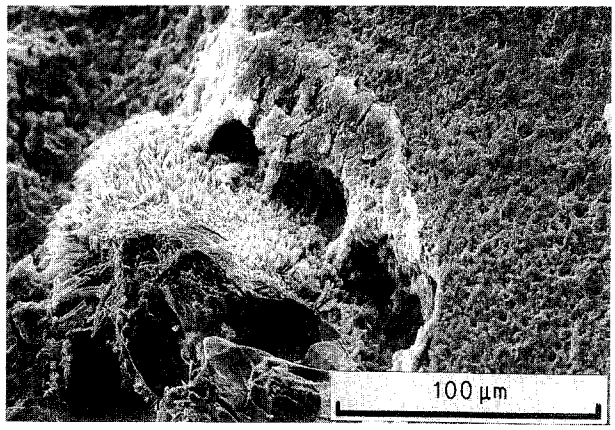

Figure 9 Surface morphology of LAS after a long anodic polarization time.

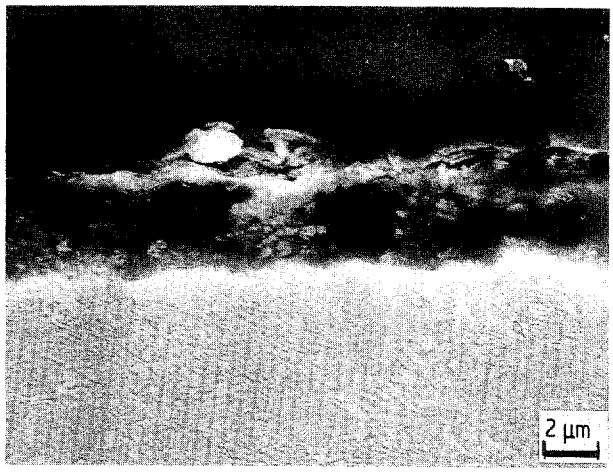

Figure 10 Cross-section of the corrosion product layer on the surface.

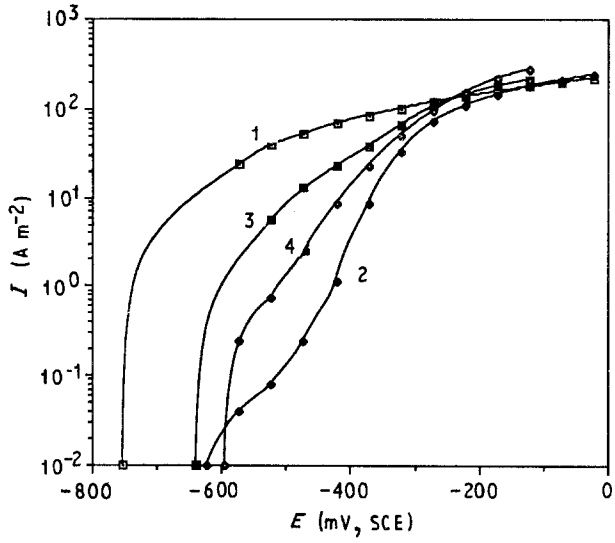

Figure 11 Anodic polarization curves in 0.1 M Na_2SO_4 solution at 25 °C. 1, 1045 steel, deaerated; 2, LAS, deaerated; 3, 1045 steel, open to the air; 4, LAS, open to the air.

which has a loose corrosion product layer about 4 μm thick. Energy dispersive X-ray analysis revealed that the chromium content in the layer was about 9.6%, while the average chromium content of LAS underneath was below 4%. It is concluded that this is a result of preferential dissolution of iron from the surface.

Fig. 11 shows anodic polarization curves of LAS and 1045 steel in 0.1 M Na_2SO_4 solution. Again the LAS shows higher corrosion potentials and lower

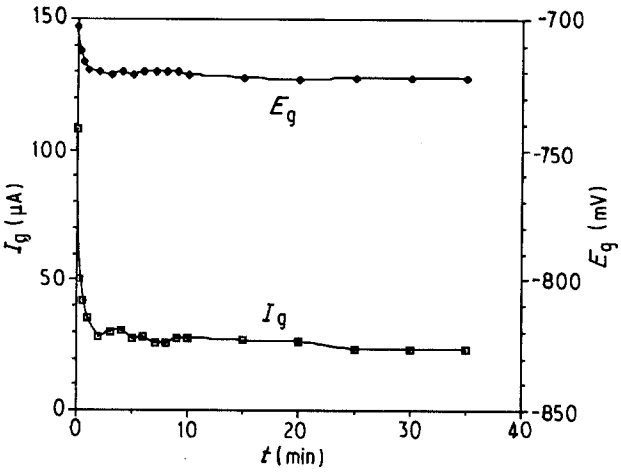

Figure 12 Galvanic potential and galvanic current transients, in 0.1 M $NaSO_4$, pH 4, 25 °C, deaerated.

anodic current densities both in deaerated solution and in the solution open to the air. The corrosion current of the LAS sample in 0.1 M Na_2SO_4 is lower than that of 1045 steel, which is different from the situation in 0.1 M H_2SO_4 solution.

Fig. 12 shows the changes of galvanic potential and galvanic current with time, for a LAS sample and a 1045 steel sample of equal surface area in 0.1 M Na_2SO_4 solution (pH = 4). The potential and current reached their stable values quickly. The galvanic potential is close to the corrosion potential of 1045 steel, which reveals that the couple was cathodically controlled and that the anodic dissolution of the couple occurred mainly on the surface of the anode–1045 steel. The result also suggests that there may be a galvanic coupling behaviour among the cathodic inclusions, the sections enriched in chromium and the sections depleted in chromium.

Fig. 13 indicates that the corrosion and passivation behaviour of LAS was similar to that of 1045 steel in 0.5 M NaOH solution. However, the transpassive potential of LAS was about 500 mV lower than that of 1045 steel, which was obviously due to the oxidation of Cr^{3+} to Cr^{6+}

4. Discussion

During the laser remelting process, chromium boride particles are partially melted into the surface layer. Chromium and boron atoms in the melted layer diffuse outward from the particles. However, the laser treatment time is too short for these elements to distribute uniformly, and concentration gradients of chromium and boron are established in the solidified surface layer. Near chromium boride particles, where there is a high boron concentration, iron borides may be formed.

The experimental results indicate hydrogen evolution is accelerated on the laser-alloyed surface. Boron cannot affect hydrogen evolution because the average boron content in the surface layer is less than 0.5 wt %, and it was reported that boron has a relatively high hydrogen overpotential [9]. It has also been reported that the boride of iron does not promote the hydrogen evolution reaction [10], although the increase in the chromium content may affect the cathodic reaction to some extent [11]. Therefore, the chromium boride particles, as cathodic components, play an important role in facilitating hydrogen evolution.

When the sample is immersed in 0.1 M H_2SO_4 solution, both iron and chromium are dissolved from the surface into solution. The equilibrium potential for the dissolution of chromium is much lower than that of iron, which may be the reason for the sharp decrease in the corrosion potential at the initial stage. The distribution of chromium in the surface layer is uneven, so different portions which have different chromium contents on the surface may show different electrochemical behaviour. From Fig. 14 [7], it can be seen that in dilute sulphuric acid solution, the corrosion potential and passive potential of Fe–Cr alloy decrease as the chromium content increases. However, under the present experimental conditions, the entire alloy surface must be at the same potential, which is about 60 millivolts higher than the corrosion potential of carbon steel, due to the influence of the cathodic inclusions. The location of that potential, E_0, is illustrated in Fig. 14. At such a potential, the portions with high chromium content on the surface layer will be

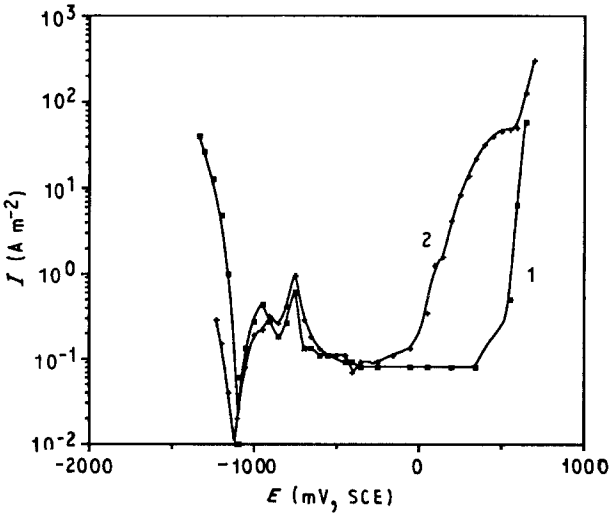

Figure 13 Polarization curves in 0.5 M NaOH solution at 25 °C. 1, 1045 steel; 2, LAS.

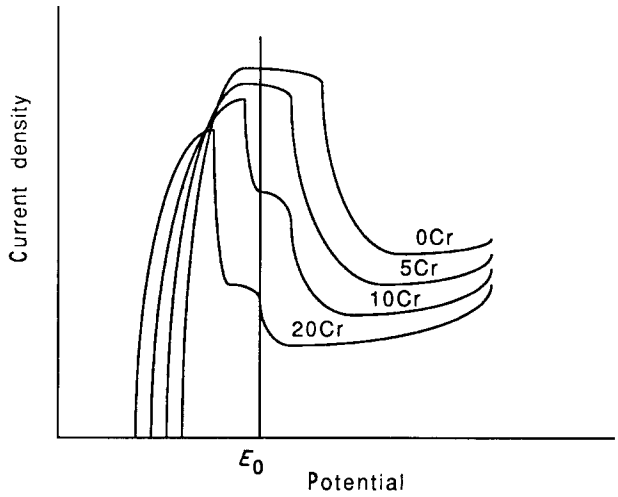

Figure 14 Polarization curves of Fe–Cr alloys with various chromium contents in dilute H_2SO_4 solution.

passivated locally, and the portions with low chromium content remain in active dissolution. The lower the chromium content, the higher the dissolution rate. In microscopic dimension, there is a fluctuating distribution of chromium among the microdendrites, which may be responsible to the formation of the small pits.

Iron and chromium in the surface layer will not dissolve at the same rate. In dilute sulphuric acid the partial dissolution rate of chromium in Fe–Cr binary alloys decreased greatly compared to that of pure chromium, while the partial dissolution rate of iron in the alloy was higher than that of pure iron [12]. As a result, in Fe–Cr alloys the partial dissolution rate of iron is higher than that of chromium. Therefore, on the active dissolving portion, where the chromium content is too low to passivate the surface, preferential dissolution of iron takes place with an accumulation of chromium on the surface. It was suggested [12] that the preferential dissolution may heal the weakest sections of the surface, as if placing additional patches on them by accumulating the more stable component. As the chromium content increases at the corroding sites, the total dissolution rate gradually decreases. The pits cannot develop steadily. At other active sites new pits will occur, and the pits may be incorporated with one another. Finally pitting will be substituted by general corrosion. Although there are some small passive portions in the beginning, they cannot remain in the stable passive state because the size of the passive portions is only about 10–20 μm, and the local potential and current must be unstable. During this period the corrosion potential of the surface layer increases slowly, because of the retardation of anodic dissolution and gradual formation of a corrosion product layer.

The variations of corrosion potential and the corresponding dissolution current are illustrated in Fig. 15. E_c is the equilibrium potential of the hydrogen evolution reaction. To simplify the illustration, suppose that the equilibrium potential for dissolution of Fe–Cr alloys with various chromium contents in the test solution has a constant value, E_a. Curves a1 and c1 stand for the partial polarization curves of the anodic dissolution of iron and hydrogen evolution reaction on the surface of iron, respectively. When chromium boride inclusions are introduced into the surface, the cathodic reaction is accelerated and the partial polarization curve of the hydrogen evolution reaction on the alloyed surface becomes c2, leading to an increase in dissolution current and corrosion potential at chromium-depleted portions. However, the partial polarization curve of the anodic reaction will also change from a1 to a2, due to the retardation of anodic dissolution and the establishment of a corrosion product layer. After the surface is covered with a layer of corrosion products, the corrosion potential reaches a stable value, E_2. At active corrosion potential, this corrosion product layer may be composed of mainly oxides and hydroxides of iron and chromium, which act as a weak barrier [13] for dissolution of the alloy.

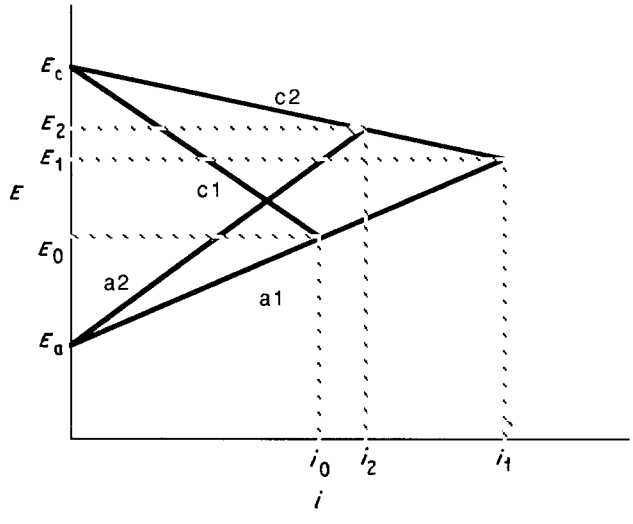

Figure 15 Illustration of corrosion potential and current changes in the corrosion process.

Chromium boride particles on the surface as cathodic components promote hydrogen evolution in the corrosion process and result in a higher corrosion potential. It is possible that hydrogen evolution and dissolution of the regions around the inclusions lead to their cracking and stripping (Fig. 9).

The anodic current density of the laser-alloyed surface is lower than that of 1045 steel at the same anodic polarization potential. This is understandable, because the chromium-enriched islands, which have lower corrosion rate, occupy a fraction of the surface. In deaerated 0.1 M Na_2SO_4 solution, the cathodic reaction proceeds very slowly, so the corrosion behaviour of the alloy is decided by its anodic behaviour and the alloyed surface shows a lower corrosion rate.

In summary, chromium boride inclusions play an important role in the corrosion process of the laser-alloyed surface. The uneven distribution of chromium results in different corrosion rates during early dissolution. However, general corrosion tends to occur due to the preferential dissolution of iron. It seems that boron does not affect the corrosion behaviour significantly, because the average boron content in the surface layer is only 0.37 wt %.

5. Conclusions

1. Chromium boride inclusions in the laser-alloyed surface behave as cathodic components, promoting hydrogen evolution and controlling the cathodic behaviour of the alloy.

2. Chromium is spread unevenly throughout the surface layer, which determines the anodic behaviour of the alloy. During early corrosion, pits occurred at active sites depleted in chromium.

3. Iron is dissolved preferentially from the surface in 0.1 M H_2SO_4 solution. A loose corrosion product film is formed that is enriched in chromium. This corrosion product film gives low corrosion protection, allowing the alloy to be actively corroded.

4. In neutral and basic solutions, the corrosion behaviour of the laser-alloyed surface is close to that of the matrix 1045 steel.

Acknowledgements

The authors are grateful to Dr M. Bamberger and his colleagues for the supply of the laser-alloyed material.

References

1. L. S. LYAKHOVICH, *et al., Radiation. Metallored. Term. Obrab. Met.* **11** (1985) 12.
2. Y. M. LAKHIN, Y. O. KOGAN and A. V. BURYAKIN, *ibid.* **11** (1985) 9.
3. A. G. GRIGOR'YANTS, *Electrochem. Ind. Process. Biol.* **5** (1982) 35.
4. A. G. GRIGOR'YANTS, *et al. ibid.* **2** (1984) 46.
5. M. BAMBERGER, M. BOAZ and G. SHAFIRSTIEN, unpublished work (1989).
6. P. G. MOORE and E. McCAFFERTY, *J. Electrochem. Soc.* **128** (1981) 1391.
7. K. SHIOBARA, Y. SAWADA and S. MORIOKA, *J. Jpn Inst. Metals* **27** (1963) 419.
8. P. CADET, M. KADDEM and H. TAKENOUTI, "Passivity of Metals and Semiconductors" (Elsevier Science, Amsterdam, 1983) p. 311.
9. R. RAMSHAM, *et al. J. Electrochem. Soc.* **134** (1987) 2133.
10. V. S. RAJA, KISHORE and S. RANGANATHAN, *Corros.* **44** (1988) 263.
11. M. NAKA, K. HASHIMOTO and T. MASUMOTO, *ibid.* **32** (1976) 147.
12. Y. M. KOLOTYRKIN, *Electrochem. Acta* **25** (1980) 89.
13. M. NAKA, K. HASHIMOTO and T. MASUMOTO, *J. Non-Cryst. Solids*, **31** (1979) 355.

Received 6 February
and accepted 14 June 1991